

This is the **submitted version** of the journal article:

Wang, Zhe; Zhu, Zaichun; Cao, Sen; [et al.]. «Estimating Canopy Leaf Angle from Leaf to Ecosystem Scale : A Novel Deep Learning Approach Using Unmanned Aerial Vehicle Imagery». New Phytologist, Vol. 247, Issue 1 (July 2025), p. 408-425. DOI 10.1111/nph.70197

This version is available at <https://ddd.uab.cat/record/318443>

under the terms of the  ^{IN}
COPYRIGHT license

Estimating Canopy Leaf Angle from Leaf to Ecosystem Scale: A Novel Deep Learning Approach Using Unmanned Aerial Vehicle Imagery

Zhe Wang^{1,2}, Zaichun Zhu^{1,2}*, Sen Cao^{1,2}, Josep Peñuelas^{3,4}, Da Zeng^{1,2}, Dajing Li^{1,2}, Weiqing Zhao^{1,2}, Yaoyao Zheng^{1,2}, Jiana Chen^{1,2}, Pengjun Zhao^{1,2}

¹ School of Urban Planning and Design, Shenzhen Graduate School, Peking University, Shenzhen, China

² Key Laboratory of Earth Surface System and Human-Earth Relations, Ministry of Natural Resources of China, Shenzhen Graduate School, Peking University, Shenzhen, China

³ CSIC, Global Ecology Unit, CREAF-CSIC-UAB, Bellaterra (Catalonia), Spain

⁴ CREAF, Cerdanyola del Vallès (Catalonia), Spain

* Correspondence to: Zaichun Zhu (zhu.zaichun@pku.edu.cn)

Abstract: Leaf angle distribution (LAD) impacts plant photosynthesis, water use efficiency, surface temperature, and ecosystem primary productivity, which are crucial for understanding surface energy balance and climate change responses. Traditional LAD measurement methods are time-consuming and often limited to individual sites, hindering effective data acquisition at the ecosystem scale and complicating the modeling of canopy LAD variations. In this Technical Advance, we present a deep learning (DL) approach that is more affordable, efficient, less labor-intensive, and automated compared to traditional methods for estimating LAD. The UAV LAD-DL method uses unmanned aerial vehicle (UAV) images (4000×3000 pixels) processed with structure-from-motion (SfM) point cloud algorithms and the Mask R-CNN deep learning network. Validation at the single-

leaf scale, with manual measurements for three plant species, demonstrated high accuracy (*Pachira glabra*: $R^2 = 0.87$ ($p < 0.001$), $RMSE = 7.61^\circ$; *Ficus elastica*: $R^2 = 0.91$ ($p < 0.001$), $RMSE = 6.72^\circ$; *Schefflera macrostachya*: $R^2 = 0.85$ ($p < 0.001$), $RMSE = 5.67^\circ$). For individual tree species, 20,616, 1,478, 2,404, and 3,653 leaf inclination angles (LIAs) were estimated in a 30×30 m plot for *Melodinus suaveolens*, *Daphniphyllum calycinum*, *Endospermum chinense*, and *Tetracera sarmentosa*, with LAD frequency ranges of 5° to 50° , 10° to 45° , 5° to 35° , and 5° to 45° , respectively. At the ecosystem scale, 57,032 LIAs were estimated in the sample plot, with a higher LAD frequency range of 10° to 55° and a mean LIA of 36.54° . The UAV LAD-DL method efficiently estimates LAD across scales, providing critical structural information for ecosystem modeling, including species-specific leaf strategies and their effects on light interception and photosynthesis in diverse forests.

Keywords: Leaf angle distribution; Ecosystem; Unmanned aerial vehicle; Deep learning

1 INTRODUCTION

Global change can affect plant growth by influencing plant structure and physiology (Ehbrecht et al., 2021; Hai, Shangguan, Peng, & Deng, 2023; Zeng et al., 2023). Leaf inclination angle (LIA), as an important parameter characterizing plant structure and function, is crucial for biophysical function, crop breeding, global change ecology, and other studies (Yang et al., 2023). LIA describes the inclination angle of leaves relative to the horizontal plane (Li, Fang, & Zhang, 2023; Wilson, 1959). Leaf angle distribution (LAD) is defined as the proportion of leaf area per unit of leaf zenith angle or azimuth angle (Liu et al., 2019). LAD has been found to impact surface temperatures, photosynthetic processes, and hydrological activities of vegetation canopies (Baldocchi, Wilson, & Gu, 2002; Emmel et al., 2020; Mantilla-Perez & Fernandez, 2017; Myneni et al., 1986; Sellers, 1985;

Vicari, Pisek, & Disney, 2019), and can vary greatly depending on factors such as light, growing season, canopy height, and tree species (Hosoi & Omasa, 2009; F. Li et al., 2023; Meunier et al., 2022; Omasa, Hosoi, & Konishi, 2007; Raabe, Pisek, Sonnentag, & Annuk, 2015). Studying the effects of LAD on light, water, and heat is crucial for better understanding vegetation's response to environmental changes.

LAD's field measurement methods include both direct and indirect methods. Direct methods involve physical contact with the leaf and manual measurement of LAD using tools such as inclinometers, protractors, and three-dimensional (3D) digitizers (Falster & Westoby, 2003; Lang, 1973), though these methods are often labor-intensive, time-consuming, and limited to plants with short stature (Kimes & Kirchner, 1983; Lang, 1973; Lugg, Youngman, & Hinze, 1981; Shell, Lang, & Sale, 1974). Indirect methods include leveled photography, light detection and ranging (LiDAR), and stereo imaging. Leveled photography methods use a ground camera or an unmanned aerial vehicle (UAV) to take leveled photos of the canopy side, and estimate the LAD by image analysis of leaves perpendicular to the shooting direction (McNeil, Pisek, Lepisk, & Flamenco, 2016; Pisek, Ryu, & Alikas, 2011; Ryu et al., 2010; Toda, Ishihara, Doi, & Hara, 2022). However, leveled photography methods are easily affected by leaf surface curvature and heavily rely on human-computer interaction, which can introduce significant uncertainties in estimating LAD (Raabe et al., 2015). LiDAR methods allow for non-contact measurement of structural parameters in vegetation canopy from ground-based (e.g., terrestrial laser scanning) or airborne platforms (Lei et al., 2022; Liu et al., 2019; Y. Wang & Fang, 2020). Estimates derived from LiDAR show high accuracy in measuring the LAD of both broad and curved leaves (Vicari et al., 2019). However, they are prone to deviations resulting from scattering angle, mutual occlusion of leaves, and point cloud noise.

Further, LiDAR is relatively expensive, limiting its widespread use (Bailey & Mahaffee, 2017; Paulus, 2019; Zheng & Moskal, 2012; Zhu et al., 2020). Stereo imaging methods use overlapping photographs from a camera or mobile phone to reconstruct the three-dimensional structure information of vegetation (such as corn and sugar beets) based on the principle of geometric perspective and estimate LAD (Muller-Linow, Pinto-Espinosa, Scharr, & Rascher, 2015; Qi et al., 2019; H. Wang, Zhang, Zhou, Yan, & Clinton, 2009). Stereo imaging methods require a lot of human-computer interaction to perform single leaf segmentation, and LAD estimation is limited to low vegetation canopies. Overall, current methods make it difficult to efficiently measure LAD at the ecosystem scale, limiting our understanding of how vegetation canopy structure responds to environmental changes and regulates ecosystem functioning.

In recent years, technologies such as UAVs, oblique photogrammetry, and deep learning (DL) have made measuring LAD at the ecosystem scale possible. These innovative technologies offer potential solutions to the challenges associated with traditional methods, presenting opportunities for enhanced efficiency and accuracy in LAD measurement. Integrating UAV technology with sophisticated sensors capable of recording direction and position has facilitated the efficient acquisition of high-resolution image data at plot scales (Anderson & Gaston, 2013). Utilizing SfM algorithms, recognized for their robustness and cost-effectiveness, researchers can attain precise 3D information while estimating camera parameters (Westoby, Brasington, Glasser, Hambrey, & Reynolds, 2012). Deep learning is a type of artificial intelligence that can extract complicated structural information from massive volumes of high-dimensional data (LeCun, Bengio, & Hinton, 2015). It has achieved remarkable results in image detection, image segmentation, and video analysis (Cao et al., 2023; Du & Liu, 2023; Oprea et al., 2022). The Convolutional Neural Network

(CNN) is the most commonly used deep learning method that has achieved advanced performance in many tasks for image-based phenotyping, such as species identification, leaf shape, and leaf vein (Ahmed & Hussein, 2020; Waeldchen & Maeder, 2018; Xu, Blonder, Jodra, Malhi, & Fricker, 2021). The Mask R-CNN can simultaneously perform target detection and image segmentation with the advantages of fast inference and a simplified process (K. He, Gkioxari, Dollar, & Girshick, 2020). The emergence of the Mask R-CNN has made it possible to segment single leaves from dense canopies and detect different tree species.

In this study, we propose a novel approach combining deep learning and SfM algorithms to estimate LAD from low-cost UAV images at the ecosystem scale, referred to as the UAV LAD-DL method. This method allows for efficient ecosystem-scale LAD measurements, supports multiple daily observations, and can be adapted to the single-leaf and tree species scales. We validated the method with three plant species (*Pachira glabra*, *Ficus elastica*, and *Schefflera macrostachya*) and compared the LAD estimates from UAV LAD-DL with manual and leveled photography methods. We also applied the method to four tree species (*Melodinus suaveolens*, *Daphniphyllum calycinum*, *Endospermum chinense*, and *Tetracera sarmentosa*) in sample plots. This multi-scale, species-specific approach provides crucial structural information for enhancing ecosystem models, capturing species-specific leaf strategies, and improving our understanding of light interception, photosynthesis, and overall ecosystem functioning.

2 METHODS

2.1 Study area

The Shenzhen Urban Ecological Flux Observation Station (114°35'25.61"E, 22°32'17.11"N) is located in Yangmeikeng, Dapeng New District, Shenzhen, at an elevation of 35 meters above sea level. The station has a subtropical oceanic climate with warm weather, an annual mean temperature of 22.4 °C, and abundant precipitation averaging 1933.3 mm annually. The dominant vegetation in the area consists of secondary forests, and the soil type is mainly crimson red soil with a loamy soil texture. The station has 355 frost-free days annually and 2120.5 hours of sunshine duration, receiving 4759 MJ/m² of total solar radiation annually. This site serves as a scientific experimental station with minimal human interference and represents a subtropical natural broadleaf forest ecosystem. It is equipped with numerous management facilities that support continuous intraday observation of LAD.

2.2 Data collection

UAV images of a 30m × 30m plot surrounding the Shenzhen Urban Ecological Flux Observation Station were captured on March 17, 2023 using a DJI Mavic Air 2 UAV. The UAV's camera was equipped with a fixed aperture size of f/2.8. We set the camera to automatic photo mode, allowing it to automatically adjust the shutter speed and ISO to ensure proper exposure under varying lighting conditions. The camera offered image resolutions of 12 million pixels and 48 million pixels. The optimal flight height was determined to be 2 meters above the vegetation canopy, balancing the quality of the point cloud, leaf size, and the impact of UAV propellers. In windless or light wind conditions, the UAV maintained this height above the tree canopy. The camera's pitch angle was controlled between 40° and 45° to generate high-quality stereo pairs while maintaining

work efficiency. During image acquisition, the UAV routes maintained a heading and side overlap rate of over 80%. For each waypoint (Fig. 1), three or more photographs with an 85% overlap were captured, resulting in a total of 234 images (4000×3000 pixels) to ensure the generation of high-quality point cloud data.

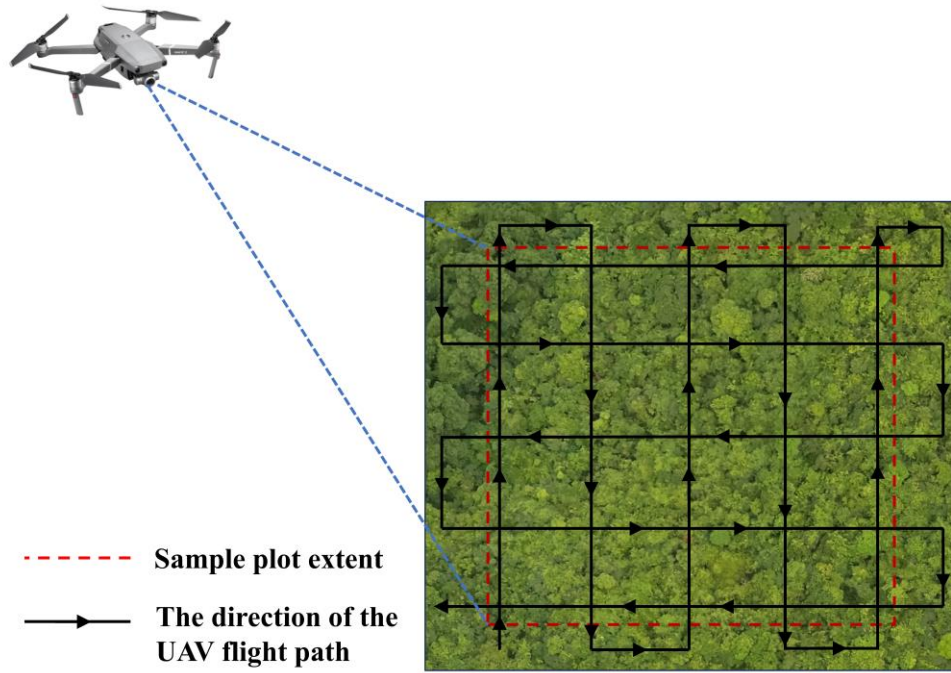


Fig. 1. UAV flight path and sample plot extent. The red dashed box indicates the spatial extent of the sample plot. The black solid line indicates the UAV flight path, and black arrows indicate the direction of the UAV flight.

Each leaf was labeled using Labelme software to construct the single-leaf segmentation dataset (Fig. 2). Labelme software is an annotation software that allows users to label objects in an image and their spatial extent (Torralba, Russell, & Yuen, 2010). We selected a representative small sample of 300 images (512×512 pixels) containing over 15000 single leaves of different tree species. These images were divided in a 4:1 ratio into training sets (208 images) and validation sets (52 images) and 40 small sample images were further chosen as test sets to assess the segmentation

accuracy of a single leaf. There is no crossover or overlap between the training, validation, and test sets to avoid data leakage.

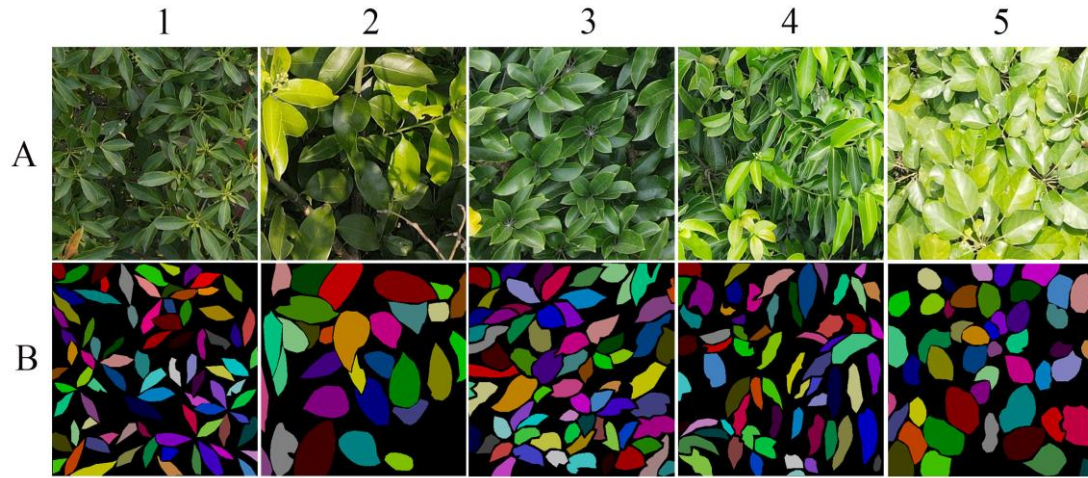


Fig. 2. Small sample images and corresponding labels. Row A represents the original small sample images. Row B represents the corresponding labels. Columns 1 to 5 represent the image and label pairs for different groups.

2.3 UAV LAD-DL method

The UAV LAD-DL method consists of four main parts, outlined in Fig. 3: 1) the segmentation of single leaves using the deep learning Mask R-CNN Network; 2) the construction of a 3D point cloud using SfM algorithms; 3) clustering the 3D point cloud into individual leaf clusters; and 4) estimating LIA and calculating the LAD for the whole plot, as well as individual tree species.

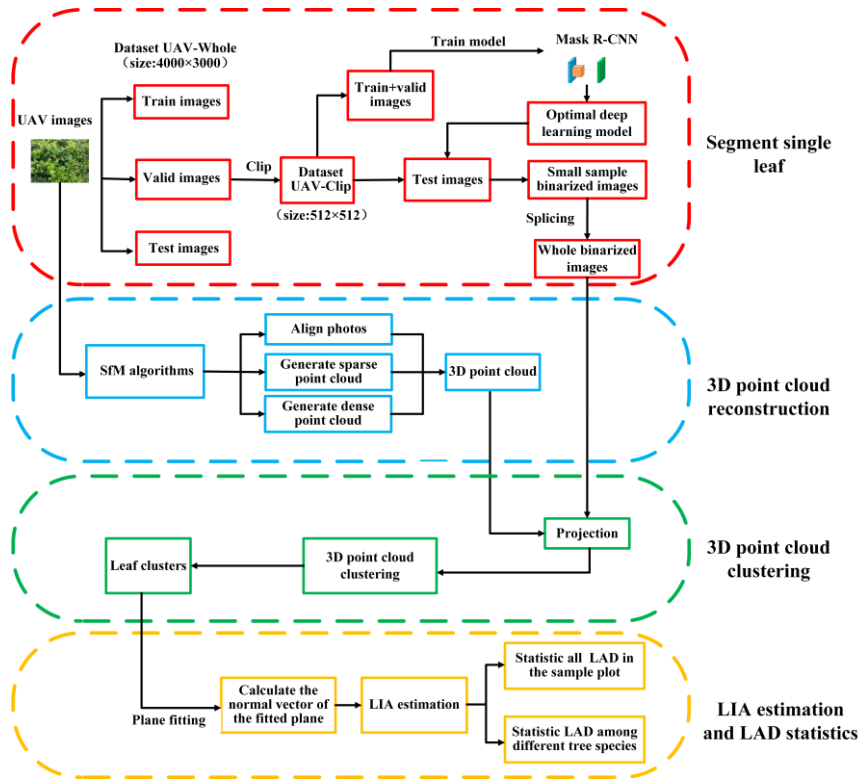


Fig. 3. Flowchart of the UAV LAD-DL method. The red dashed box indicates the process of single-leaf segmentation. The blue dashed box indicates the 3D point cloud reconstruction. The green dashed box indicates the 3D point cloud clustering. The orange dashed box indicates the process of LIA estimation and LAD statistics.

2.3.1 Single leaf segmentation

Single leaf segmentation is employed to separate point clouds of different leaves using the 2D information in the segmented image, which is applied for dividing leaf clusters in Section 2.3.3. The Mask R-CNN is a flexible and general framework for object instance segmentation (K. M. He, Gkioxari, Dollar, Girshick, & Ieee, 2017). It adds the branch of predicting target object masks to Faster R-CNN, which can efficiently detect the target objects in the image and generate high-quality segmentation masks for each instance (Ren, He, Girshick, & Sun, 2015). The Mask R-CNN network uses ResNet101 as the backbone feature extraction network, which consists of three main branches: the class branch, the box branch, and the mask branch. For leaf segmentation of various tree species,

Mask R-CNN has more advantages than other segmentation models (such as U-Net and DeepLabv3+ network) (see Supplementary Appendix A).

The architecture of the Mask R-CNN is shown in Fig. 4. The optimal Mask R-CNN deep learning model is trained by adjusting the parameters. The model's accuracy increases as the training set's loss value decreases. The initial loss value is 4.998. When the iteration count reaches 90, the loss value gradually stabilizes and remains around 0.20. At epoch 98, the training set's loss reaches a minimum of 0.193. The deep learning framework employed in this study is TensorFlow, using Python version 3.7. The model is trained at 100 epochs, starting with an initial learning rate of $1e^{-5}$, and a batch size of 4. The optimal deep learning model was used to predict the small sample images in the test sets and obtain the instance segmentation of a single leaf. The binarization process was performed with values of the leaf region (1) and background region (0). Finally, the binarized small sample image was stitched into a 4000×3000 pixel.

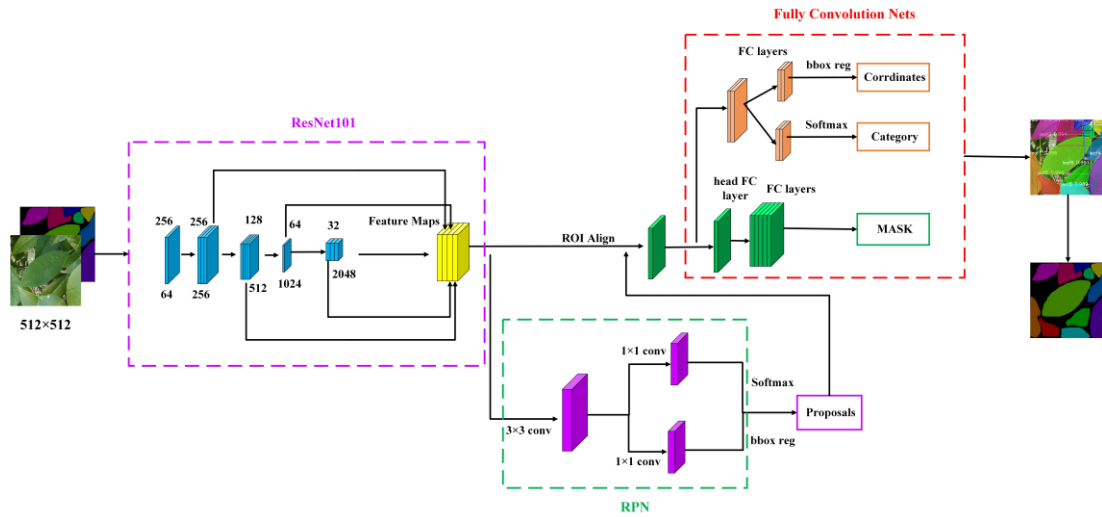


Fig. 4. Architecture of Mask R-CNN network. The purple, green, and red dashed boxes represent the ResNet101 network, the region proposal network (RPN), and the fully convolutional network, respectively.

2.3.2 3D Point cloud reconstruction

The 3D point cloud reconstruction is the crucial data foundation for LIA estimation and the primary data source for point cloud clustering in Section 2.3.3. Agisoft Metashape is a photogrammetric software widely used for 3D reconstruction, visualization, mapping, and surveying tasks. It uses mathematical techniques to recover the 3D traits and appearance of objects in still images, allowing the creation of professional-quality 3D content. Agisoft Metashape offers faster processing speeds than Pix4Dmapper, allowing for the rapid generation of high-precision point clouds and 3D models. It utilizes graphics processing unit (GPU) acceleration to enhance processing efficiency for large datasets. Additionally, Agisoft Metashape supports Python scripting and enables batch reconstruction of point clouds, which improves data processing efficiency and customizability. The SfM algorithm reconstructs point clouds of sparse scenes from a series of overlapping photos(Verhoeven, 2011). When combined with stereo matching algorithms, it is possible to fully automate the construction of detailed 3D models from photo collections. Therefore, we use the SfM algorithm in Agisoft Metashape to batch-generate 3D point clouds through a Python script. During the image alignment phase, the SfM algorithm can directly estimate the internal and external UAV camera parameters, which enables the projection of the 3D point cloud to 2D-pixel coordinates. Fig. 5 illustrates the two coordinate systems involved in UAV photography. The XYZ space is the world spatial coordinate system, with the Z-axis pointing towards the zenith and X (east) and Y (north) defined in the horizontal plane. The 3D point cloud generated by the Agisoft Metashape software falls in the camera spatial coordinate system (xyz). The z -axis is perpendicular to the UAV camera screen and points backward, and the x -axis and y -axis are defined in the UAV camera screen plane, where the y -axis points upward and the x -axis points to the right.

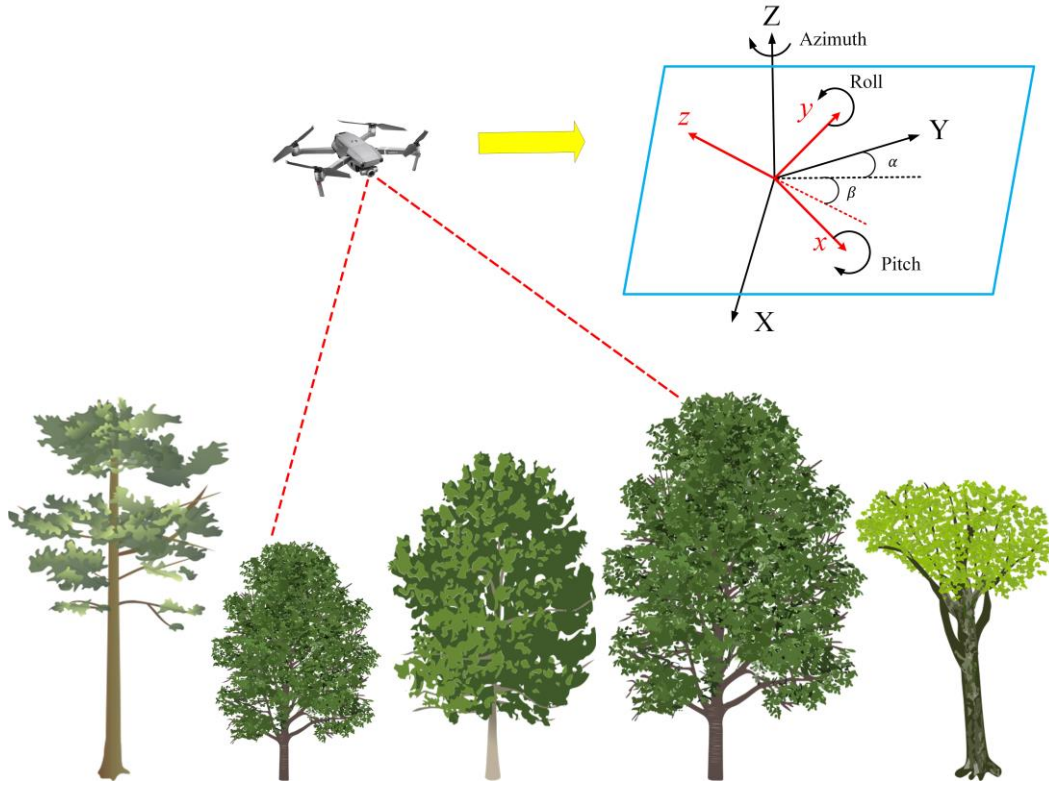


Fig. 5. Schematic diagram of the UAV camera spatial coordinate system (xyz) and the world spatial coordinate system (XYZ). β indicates the pitch angle, α indicates the azimuth angle.

2.3.3 3D point cloud clustering

The accurate fitting of the leaf plane depends on the correct division of individual leaf clusters. To divide the 3D point cloud into individual leaf clusters, the 3D point cloud was projected onto a 2D image using the internal and external UAV camera parameters estimated by the SfM algorithm. The point cloud that is not projected to the leaf region is removed. Then, the 3D point cloud is divided into individual leaf clusters based on the segmented binary images of the leaves (Fig. 6). The leaf cluster point cloud is the data source for the leaf plane fitting in Section 2.3.4.

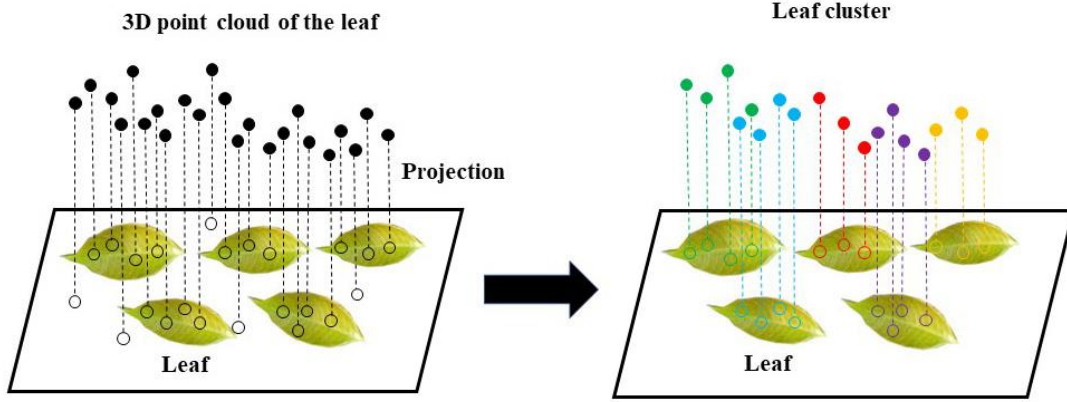


Fig. 6. Divide the 3D point cloud into leaf clusters. Black solid dots indicate the original 3D point cloud and colored solid dots indicate the clustered leaf cluster point cloud.

2.3.4 Leaf inclination angle estimation and statistics

A plane fit is performed to the 3D point cloud of each leaf cluster to obtain the inclination of each leaf plane. The leaf planes are fitted with the following equations:

$$\min_{c, \|n\|=1} \sum_{i=1}^N ((p_i - c)^T n)^2 \quad (1)$$

$$c = \frac{1}{N} \sum_{i=1}^N p_i \quad (2)$$

where p_i is the 3D point within each leaf cluster, c denotes the mean point, and N denotes the total number of 3D points within each leaf cluster. n is the normal vector of the fitting plane in the camera coordinate system.

The camera coordinate system (xyz) is converted to the world spatial coordinate system (XYZ) using the pitch angle θ_p and azimuth angle φ_p recorded in the UAV image, as shown in equation (3).

$$\begin{pmatrix} X \\ Y \\ Z \end{pmatrix} = \begin{pmatrix} \cos \varphi_p & \sin \varphi_p & -\sin \varphi_p \\ -\sin \varphi_p & \cos \varphi_p & \cos \varphi_p \\ 0 & \cos \theta_p & -\sin \theta_p \end{pmatrix} \begin{pmatrix} x \\ y \\ z \end{pmatrix} \quad (3)$$

where $n' = (X, Y, Z)$ is the normal vector of the fitted plane of the leaf in the world spatial coordinate system.

The LIA is the angle between the normal vector of the fitting plane and the zenith vector and is calculated as shown in equation (4):

$$\theta_L = \begin{cases} \arccos \frac{n' \cdot v}{\|n'\|}, & n' \cdot v \geq 0 \\ \pi - \arccos \frac{n' \cdot h}{\|n'\|}, & n' \cdot v < 0 \end{cases} \quad (4)$$

where $v = (0,0,1)$, the absolute vertical vector in the world spatial coordinate system, and $h = (0,1,0)$, the north vector of the horizontal plane in the world spatial coordinate system.

Finally, LAD was estimated for different tree species and the entire sample plot.

2.4 Segmentation accuracy and leaf inclination angles accuracy evaluation

We conducted a comparative analysis between the segmentation outcomes produced by the Mask R-CNN for individual leaves and their corresponding visual interpretations to evaluate segmentation accuracy, using various quantitative metrics (Kappa coefficient, F1 score, Recall, and mean intersection over union (mIOU)) (see Supplementary Appendix B). The Kappa coefficient serves as a standard measure of classification accuracy. Recall represents the probability of a positive sample being correctly identified among all positive samples. The F1 score, the harmonic mean of Precision and Recall, offers a comprehensive assessment of segmentation performance. Furthermore, mIOU is an essential metric for evaluating image segmentation precision and the intersection over union (IOU) is computed for each category.

We also conducted a leaf-to-leaf validation comparing LIAs estimated using the UAV LAD-DL method with manual measurements. Three metrics were employed to evaluate the estimation

accuracy of LIAs: Root Mean Squared Error (RMSE), R^2 , and the two-sample Kolmogorov-Smirnov (K-S) test. The K-S test was applied to assess whether the UAV LAD-DL method estimated LAD and the measured LAD belong to the same distribution population. The K-S test was suitable for continuous data without requiring a specific distribution assumption, making it ideal for assessing the accuracy of LAD estimation. Compared to the t-test, the K-S test is more flexible and widely applicable. If the K-S test is not passed, it indicates that the estimated LAD is different from the manually measured LAD (see Supplementary Appendix C).

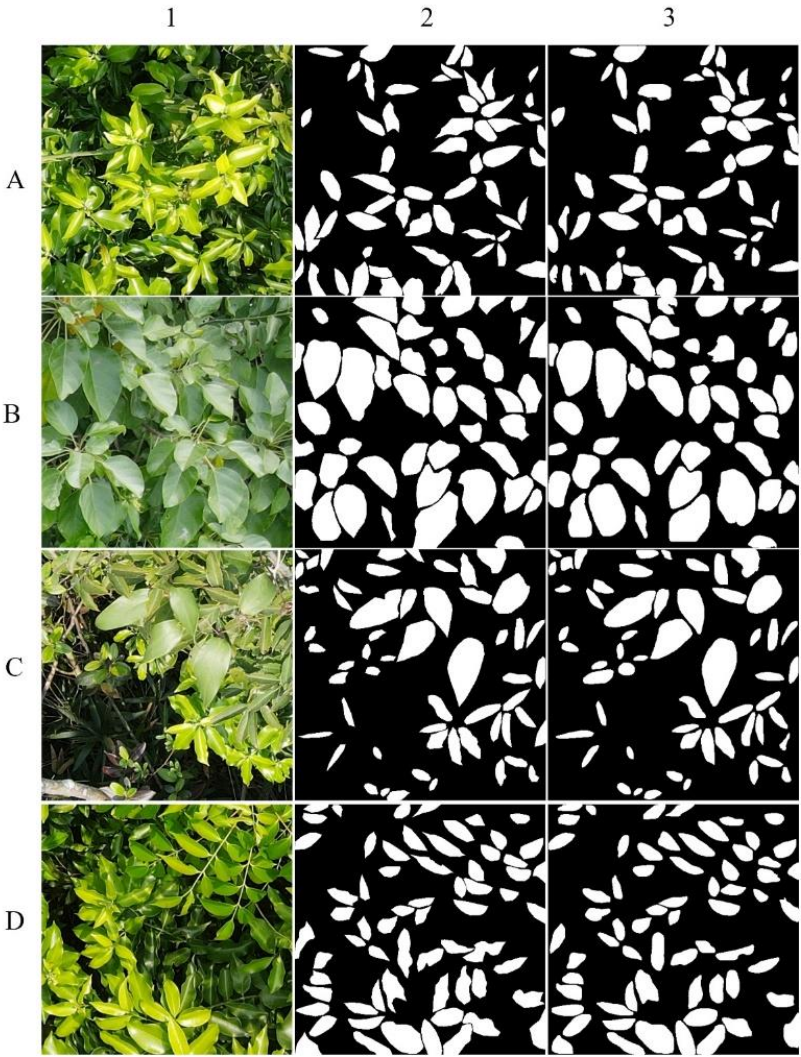
3 RESULTS AND DISCUSSION

3.1 Segmentation accuracy evaluation of single leaves

We selected 40 groups of small sample images and compared them to segmentation results derived from visual interpretation. The segmentation accuracy was assessed both visually and quantitatively. For visual segmentation (Fig. 7), the UAV LAD-DL method is better for single-leaf segmentation with smooth leaf edges and regular shapes. We also compared the segmentation performance of the UAV LAD-DL method under different shadow conditions. The UAV LAD-DL method achieved effective segmentation in both shallow and medium shadow regions (see Fig. S1 and Supplementary Appendix D). Overall, the UAV LAD-DL method excels in single-leaf segmentation, closely approximating results obtained through visual interpretation (Table 1). As shown in Fig. 8, the average Kappa coefficient, F1 score, Recall, and mIOU for the 40 groups of small sample images are 0.856, 0.887, 0.879, and 0.868, respectively. These results indicate that the UAV LAD-DL method generally achieves high accuracy in single-leaf segmentation.

Table 1 Four segmentation accuracy evaluation metrics for different image groups

Image Group	Kappa coefficient	F1 score	Recall	mIOU
A	0.82	0.862	0.829	0.838
B	0.815	0.895	0.861	0.831
C	0.863	0.896	0.884	0.874
D	0.863	0.903	0.875	0.873



277 Fig. 7. Leaf segmentation results in small sample images. Column 1 represents the original small
278 sample image. Column 2 represents the binary image segmented by visual interpretation. Column 3
279 represents the binary image segmented by the UAV LAD-DL method. The labels A-D represent the
280 different image groups.

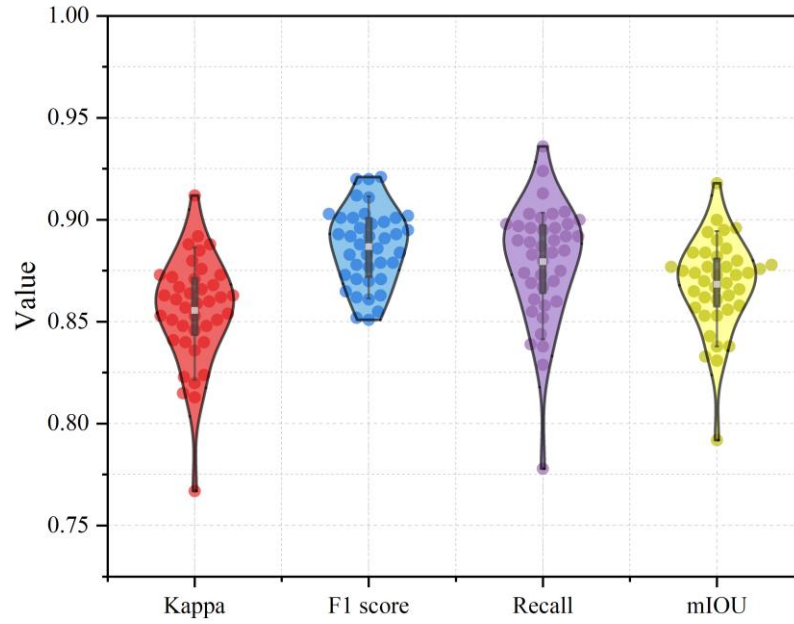


Fig. 8. Violin plot of leaf segmentation accuracy metrics (Kappa, F1 score, Recall, and mIOU).

White boxes indicate mean values, whereas solid circles indicate raw values. The box range indicates the 25% and 75% quartiles, and the whisker range indicates the 10% and 90% quartiles.

3.2 Leaf-to-leaf validation

We chose three plant species (*Pachira glabra*, *Ficus elastica*, and *Schefflera macrostachya*) with different leaf sizes, textures, and traits from the campus of Peking University Shenzhen Graduate School (Shenzhen, China) to assess the effectiveness and accuracy of the UAV LAD-DL method. We measured true LIA using a smartphone inclinometer app (70 Degree: Smart Protractor) to compare the UAV LAD-DL method to manual measurements. In addition, we compared the accuracy of the UAV LAD-DL method with the leveled photography method for *Pachira glabra* and *Ficus elastica*. However, leveled photography was not compared to *Schefflera macrostachya* due to its dense foliage, consequently making it challenging to use the leveled photography method.

The leveled photography method (*Pachira glabra*: $P=0.414$, $D=0.149$; *Ficus elastica*: $P=0.998$, $D=0.068$) passed the K-S test in both plant species, indicating that the LAD estimates from the leveling photography method conformed to the same distribution as the manual measurements. The

UAV LAD-DL method passed the K-S test in the two plant species (*Ficus elastica*: $P=0.283$, $D=0.169$; *Schefflera macrostachya*: $P=0.131$, $D=0.2$), but not *Pachira glabra* ($P=0.016$, $D=0.244$, suggesting that the LIA estimates from the UAV LAD-DL method slightly differed from manual measurements in *Pachira glabra*. However, the mean leaf inclination angle (MLIA) and standard deviation (SD) of *Pachira glabra* estimated by the UAV LAD-DL method (MLIA= 51.09° , SD= 13.25°) were consistent with the manual measurements (MLIA= 45.15° , SD= 12.86°). In *Ficus elastica* and *Schefflera macrostachya*, the MLIA of UAV LAD-DL method (*Ficus elastica*: MLIA= 31.7° , SD= 18.18° ; *Schefflera macrostachya*: MLIA= 67.98° , SD= 11.39°) and manual measurements (*Ficus elastica*: MLIA= 27.79° , SD= 17.53° ; *Schefflera macrostachya*: MLIA= 65.06° , SD= 12.48°) differed by 3.91° and 2.92° , respectively (see Supplementary Appendix E). For *Pachira glabra* and *Ficus elastica*, the leveled photography method outperforms the UAV LAD-DL method in terms of R^2 and RMSE (Fig. 9). However, the former estimates fewer LIA measurements than the latter. Overall, the UAV LAD-DL method has high LIA estimation accuracy in three plant species (*Pachira glabra*: $R^2=0.87$ ($p<0.001$), RMSE= 7.61° ; *Ficus elastica*: $R^2=0.91$ ($p<0.001$), RMSE= 6.72° ; *Schefflera macrostachya*: $R^2=0.85$ ($p<0.001$), RMSE= 5.67°). Besides, we compared the LIA extraction rate between the UAV LAD-DL method and the leveled photography method (Fig. S2). For the same UAV image, the LIA extraction rate of the UAV LAD-DL method (84.1%) is significantly higher than the leveled photography method (5.7%) (see Supplementary Appendix F).

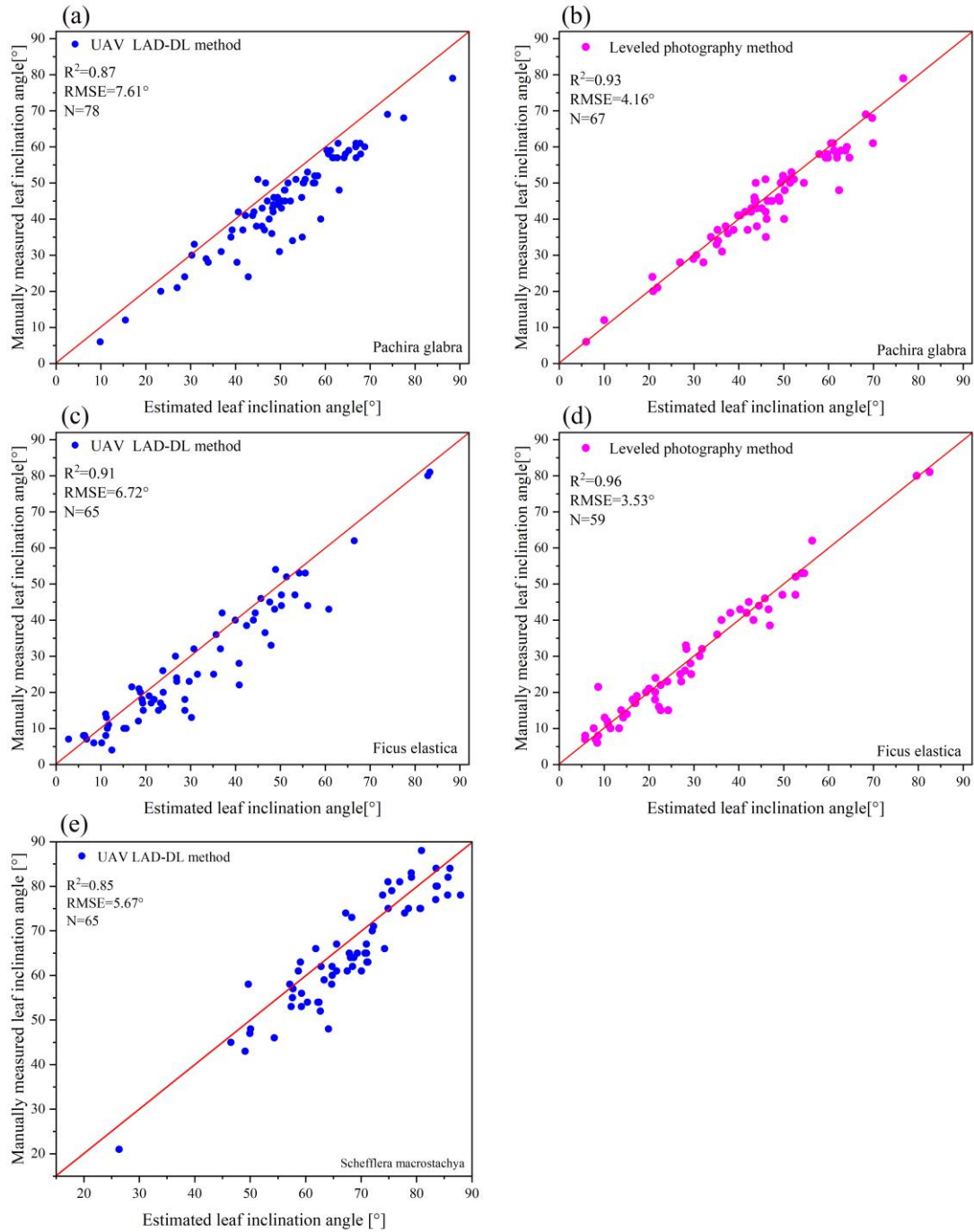


Fig. 9. Leaf-to-leaf validation between LIA estimated by different methods and manual measurements in three plant species. (a), (c), and (e) show the comparison of the UAV LAD-DL method with manual measurements. (b) and (d) show the comparison of the leveled photography method with manual measurements.

3.3 Estimation of LAD from UAV images

In Groups A, B, C, and D of UAV images, the UAV LAD-DL method estimated 1020, 883, 771, and 1212 LIAs, respectively (Fig. 10). Across the four sets of UAV images, the higher frequency ranges of LAD were concentrated primarily between 5° to 35° (A: 76.7% of all frequencies), 30° to 70° (B: 75.2%), 10° to 50° (C: 71.9%), and 0° to 25° (D: 92.1%). The MLIA had a great variation in the UAV images of different groups. The highest MLIA was found in group B (50.47°) and the lowest in group D (12.41°). The MLIA in groups A (24.04°) and C (34.92°) was below 45° . The MLIA of group B was 26.43° , 15.55° , and 38.06° higher than the other three groups (A, C, and D), respectively. In addition, the UAV LAD-DL method can map the extracted individual LIAs to the leaves in the image (as shown in column 3 of Fig. 10), facilitating the study of LIA variations at the single-leaf scale. For the binarized image of group A, some leaves in the far-view area were not segmented. The main reason was that the height of the vegetation canopy in the image varies greatly, resulting in smaller leaves in the far-view region, which was not conducive to segmentation.

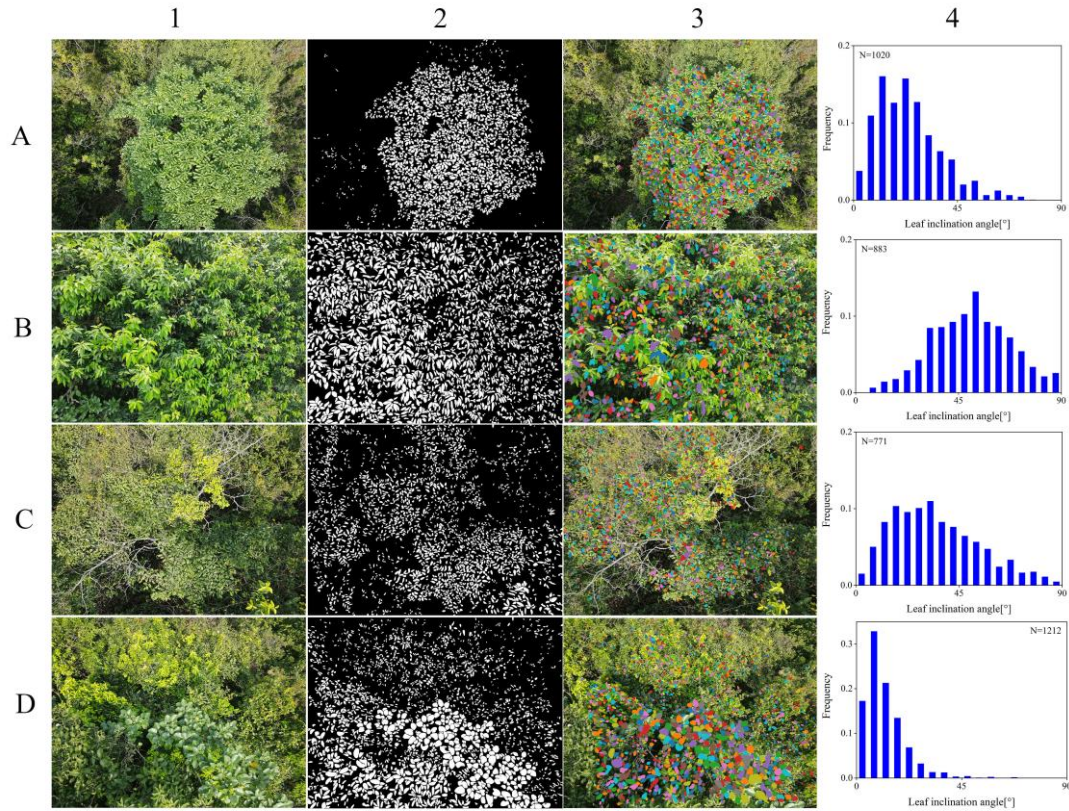


Fig. 10. Estimation of LAD from UAV images. Columns 1 and 2 represent the original UAV image and the segmented binarized image, and columns 3 and 4 represent the projection point position of the 3D point cloud and the estimated LAD. A to D represent different groups of UAV images.

In the UAV images groups E to H (Fig. 11), for *Melodinus suaveolens* (E: MLIA=31.05°; F: MLIA=23.87°; G: MLIA=24.8°; H: MLIA=36.66°), 101,127,368, and 330 LIAs were estimated, and the frequency ranges of LAD were concentrated at 15° to 40°, 5° to 30°, 5° to 35°, and 10° to 50°, respectively. 183,105,69, and 60 LIAs were estimated for *Daphniphyllum calycinum Benth* (E: MLIA=28.02°; F: MLIA=22.18°; G: MLIA=26.52°; H: MLIA=31.77°), and the high frequencies of LAD were concentrated at 10° to 45°, 5° to 35°, 10° to 40°, and 10° to 35°, respectively. The frequency ranges of LAD were concentrated at 0° to 20°, 0° to 25°, 5° to 30°, and 5° to 35° for the 35, 74, 296, and 290 LIAs estimated for *Endospermum chinense* (E: MLIA=19.67°; F: MLIA=11.33°; G: MLIA=19.05°; H: MLIA=24.77°), For *Tetracera sarmentosa* (E: MLIA=29.12°;

F: MLIA=22.56°; G: MLIA=24.42°; H: MLIA=34.25°), 444, 423, 150, and 268 LIAs were estimated, and the frequencies of LAD were concentrated at 20° to 40°, 5° to 30°, 5° to 40°, and 15° to 50°, respectively.

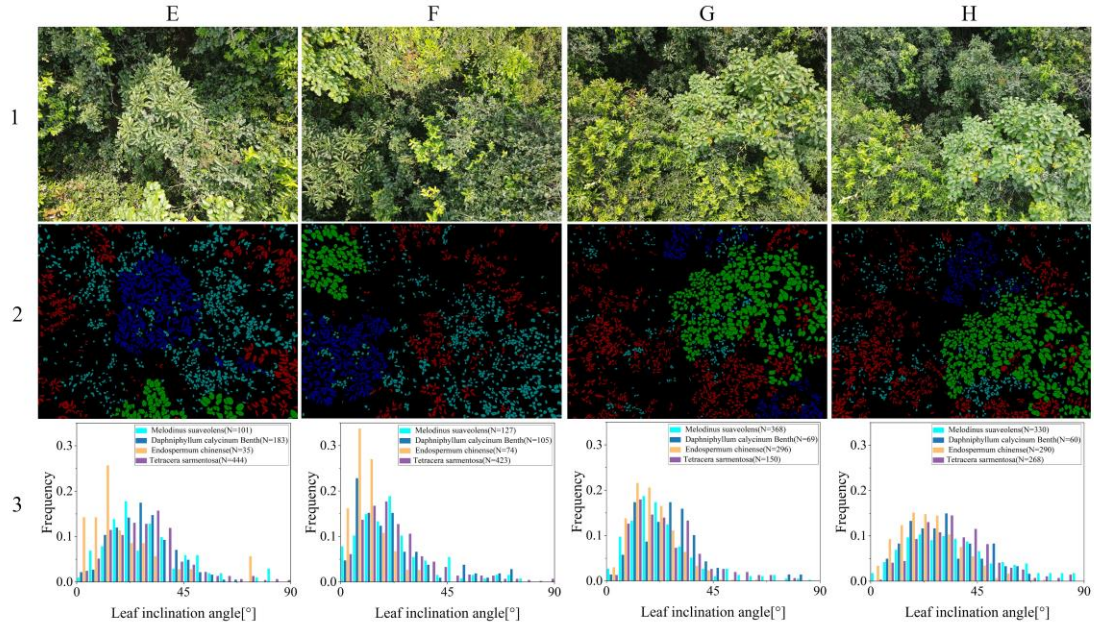


Fig. 11. LAD of different tree species. Row 1 represents the original UAV image, while row 2 represents the segmented tree species image. Row 3 represents the LAD of different tree species. E to H represent different groups of UAV images.

We also estimated 57032 LIAs in the sample plot, with higher LAD frequencies ranging from 10° to 55°(71.4% of all frequencies), and a MLIA of 36.54° (Fig. 12a). In the sample plot, for *Melodinus suaveolens* (MLIA=34.79 °), *Daphniphyllum calycinum Benth* (MLIA=31.22 °), *Endospermum chinense* (MLIA=25.4 °), and *Tetracera sarmentosa* (MLIA=30.37 °), 20616,1478,2404, and 3653 LIAs were estimated, and the higher frequencies of LAD were concentrated at 5° to 50° (75.7% of all frequencies), 10° to 45° (70.2%), 5° to 35° (70.3%), and 5° to 45° (77.6%), respectively (Fig. 12b). The MLIA of the sample plot was higher than the four tree species (5%, 17%, 43.9%, and 20.3% higher, respectively).

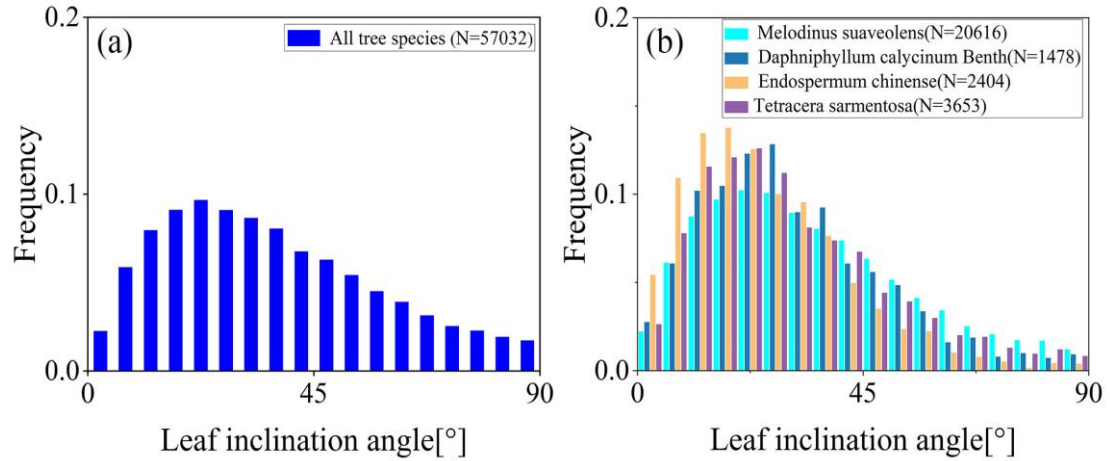


Fig. 12. LAD of four representative tree species (a) and all tree species (b) in the sample plot.

3.4 Advantages of the UAV LAD-DL method

The UAV LAD-DL method is affordable, automated, efficient, highly accurate, and requires little labor. The method is applicable at the ecosystem scale but can provide three-dimensional modeling information and accurate LIA estimates at the single-leaf and single-tree scales. Thus, the method provides fine canopy structure information within the ecosystem. Overall, the method is suitable for efficient ecosystem-scale measurements that can satisfy multiple observations within a day and be refined to single-leaf and tree species scales. Thus, this method is important for future studies on the dynamics of LAD at different temporal scales (daily scale, monthly scale, interannual scale) and spatial scales (single leaf scale, tree species scale, and ecosystem scale). Moreover, the UAV LAD-DL method is suitable for a broader range of leaf scenes than the leveled photography method, eliminates the requirement for human-computer interaction in LAD measurement, significantly broadens the scope of LAD estimation methods and mitigates subjective human errors.

3.5 Limitations and future perspectives

During the estimation process of LIA, several uncertainties arise. First, manual measurements of LIA introduce a degree of human subjectivity, particularly when dealing with small leaves or

leaves with not flat surfaces. Second, the quality of the point cloud reconstructed by the SfM algorithm can impact the accuracy of LIA measurements. Low-quality point cloud can affect the precision of the plane fitting process and lead to biased estimations of leaf plane normals (see Supplementary Appendix G). LAD is essential for ecology and forestry because it directly influences light capture efficiency, photosynthesis, and ecosystem function (see Supplementary Appendix H). Observations of LAD are crucial for understanding how ecosystems efficiently use light energy and contribute to habitat management and conservation (see Supplementary Appendix I).

The UAV LAD-DL method proposed in this study can estimate the LIA of curved leaves (see Fig. S3 and Supplementary Appendix J) and improve the accuracy of LAI estimation. When estimating LAI using hemispherical photography or light sensors, it is commonly assumed that the LAD is spherical or homogeneous at different azimuths (Jonckheere et al., 2004). However, a recent study found that LAI estimates based on measured LAD could be up to 25% higher than those where the LAD is assumed to be spherical and homogenous distribution (Stovall, Masters, Fatoyinbo, & Yang, 2021). Therefore, this study could help improve LAI estimation accuracy further. Moreover, LIA variations of up to 60 degrees have been observed throughout the day in soybeans and some desert plants, resulting from plant strategies to regulate light interception and water loss (Ehleringer & Forseth, 1980; Kao & Forseth, 1992). The UAV LAD-DL method offers the benefits of rapid measurement and enables multiple observations throughout the day. Furthermore, it provides an opportunity to investigate the intraday and seasonal dynamics of LAD and their effects on light energy allocation and resource competition, revealing the dynamic equilibrium mechanisms of

ecosystems. This method can also be applied in the future for ground validation of remote sensing LIA inversion results and for improving related models (see Supplementary Appendix K).

4 CONCLUSION

This study presents a novel approach for estimating leaf angle distribution at the ecosystem scale by integrating deep learning techniques with the SfM algorithm to analyze affordable UAV imagery, enabling efficient LAD estimation across large areas. The UAV LAD-DL method has the advantages of being affordable, efficient, highly accurate, and less labor-intensive. The method achieved high segmentation accuracy for individual leaves (Kappa coefficient=0.856, F1 score=0.887, recall=0.879, mIOU=0.868). Moreover, the method demonstrated high estimation accuracy for tree species with different leaf textures and sizes (*Pachira glabra*: $R^2=0.87$ ($p<0.001$), RMSE=7.61°; *Ficus elastica*: $R^2=0.91$ ($p<0.001$), RMSE=6.72°; *Schefflera macrostachya*: $R^2=0.85$ ($p<0.001$), RMSE=5.67°). The UAV LAD-DL method has higher applicability than the leveled photography method, and the estimation process of LAD is fully automated, greatly reducing the estimation errors caused by human subjectivity. Overall, the UAV LAD-DL method can efficiently measure LAD from single leaf to ecosystem scales and has the potential to be further refined to derive various detailed canopy structure parameters for various research proposes.

AUTHOR CONTRIBUTIONS

Zhe Wang: Conceptualization, Data curation, Formal analysis, Methodology, Software, Visualization, Writing – original draft. **Zaichun Zhu:** Conceptualization, Funding acquisition, Methodology, Supervision, Writing – review & editing. **Sen Cao:** Writing – review & editing. **Josep**

Peñuelas: Writing – review & editing. **Da Zeng:** Data curation, Formal analysis. **Dajing Li:** Data curation, Formal analysis. **Weiqing Zhao:** Data curation, Formal analysis. **Yaoyao Zheng:** Data curation, Formal analysis. **Jiana Chen:** Data curation, Formal analysis. **Pengjun Zhao:** Data curation, Formal analysis.

CONFLICT OF INTEREST STATEMENT

The authors declare that they have no known competing financial interests or personal relationships that could have appeared to influence the work reported in this paper.

ACKNOWLEDGMENTS

This study was supported by the National Natural Science Foundation of China (42271104, 42471103) and the Shenzhen Science and Technology Program (JCYJ20220531093201004, KQTD20221101093604016).

REFERENCES

- Ahmed, A., & Hussein, S. E. (2020). Leaf identification using radial basis function neural networks and SSA based support vector machine. *PLOS ONE*, 15(8). doi:10.1371/journal.pone.0237645
- Anderson, K., & Gaston, K. J. (2013). Lightweight unmanned aerial vehicles will revolutionize spatial ecology. *Frontiers in Ecology and the Environment*, 11(3), 138-146. doi:10.1890/120150
- Bailey, B. N., & Mahaffee, W. F. (2017). Rapid measurement of the three-dimensional distribution of leaf orientation and the leaf angle probability density function using terrestrial LiDAR scanning. *Remote Sensing of Environment*, 194, 63-76. doi:10.1016/j.rse.2017.03.011
- Baldocchi, D. D., Wilson, K. B., & Gu, L. H. (2002). How the environment, canopy structure and canopy

444 physiological functioning influence carbon, water and energy fluxes of a temperate broad-
 445 leaved deciduous forest-an assessment with the biophysical model CANOAK. *Tree Physiology*,
 446 22(15-16), 1065-1077. doi:10.1093/treephys/22.15-16.1065
 447 Cao, Y. Y., Zhao, Z. X., Huang, Y., Lin, X., Luo, S. Y., Xiang, B. R., & Yang, H. C. (2023). Case instance
 448 segmentation of small farmland based on Mask R-CNN of feature pyramid network with double
 449 attention mechanism in high resolution satellite images. *Computers and Electronics in*
 450 *Agriculture*, 212. doi:10.1016/j.compag.2023.108073
 451 Du, W., & Liu, P. (2023). Instance Segmentation and Berry Counting of Table Grape before Thinning
 452 Based on AS-SwinT. *Plant Phenomics*, 5. doi:10.34133/plantphenomics.0085
 453 Ehbrecht, M., Seidel, D., Annighoefer, P., Kreft, H., Koehler, M., Zemp, D. C., . . . Ammer, C. (2021).
 454 Global patterns and climatic controls of forest structural complexity. *Nature Communications*,
 455 12(1). doi:10.1038/s41467-020-20767-z
 456 Ehleringer, J., & Forseth, I. (1980). SOLAR TRACKING BY PLANTS. *Science*, 210(4474), 1094-1098.
 457 doi:10.1126/science.210.4474.1094
 458 Emmel, C., D'Odorico, P., Reville, A., Hortal, L., Ammann, C., Buchmann, N., & Eugster, W. (2020).
 459 Canopy photosynthesis of six major arable crops is enhanced under diffuse light due to canopy
 460 architecture. *Global Change Biology*, 26(9), 5164-5177. doi:10.1111/gcb.15226
 461 Falster, D. S., & Westoby, M. (2003). Leaf size and angle vary widely across species: what consequences
 462 for light interception? *New Phytologist*, 158(3), 509-525.
 463 Hai, X., Shanguan, Z., Peng, C., & Deng, L. (2023). Leaf trait responses to global change factors in
 464 terrestrial ecosystems. *Science of The Total Environment*, 898.
 465 doi:10.1016/j.scitotenv.2023.165572

466 He, K., Gkioxari, G., Dollar, P., & Girshick, R. (2020). Mask R-CNN. *IEEE Transactions on Pattern*
467 *Analysis and Machine Intelligence*, 42(2), 386-397. doi:10.1109/tpami.2018.2844175

468 He, K. M., Gkioxari, G., Dollar, P., Girshick, R., & Ieee. (2017, Oct 22-29). *Mask R-CNN*. Paper
469 presented at the 16th IEEE International Conference on Computer Vision (ICCV), Venice,
470 ITALY.

471 Hosoi, F., & Omasa, K. (2009). Detecting seasonal change of broad-leaved woody canopy leaf area
472 density profile using 3D portable LIDAR imaging. *Functional Plant Biology*, 36(10-11), 998-
473 1005. doi:10.1071/fp09113

474 Jonckheere, I., Fleck, S., Nackaerts, K., Muys, B., Coppin, P., Weiss, M., & Baret, F. (2004). Review of
475 methods for in situ leaf area index determination - Part I. Theories, sensors and hemispherical
476 photography. *Agricultural and Forest Meteorology*, 121(1-2), 19-35.
477 doi:10.1016/j.agrformet.2003.08.027

478 Kao, W. Y., & Forseth, I. N. (1992). DIRUNAL LEAF MOVEMENT, CHLOROPHYLL
479 FLUORESCENCE AND CARBON ASSIMILATION IN SOYBEAN GROWN UNDER
480 DIFFERENT NITROGEN AND WATER AVAILABILITIES. *Plant Cell and Environment*,
481 15(6), 703-710. doi:10.1111/j.1365-3040.1992.tb01012.x

482 Kimes, D. S., & Kirchner, J. A. (1983). DIURNAL-VARIATIONS OF VEGETATION CANOPY
483 STRUCTURE. *International Journal of Remote Sensing*, 4(2), 257-271.
484 doi:10.1080/01431168308948545

485 Lang, A. R. G. (1973). LEAF ORIENTATION OF A COTTON PLANT. *Agricultural Meteorology*, 11(1),
486 37-51. doi:10.1016/0002-1571(73)90049-6

487 LeCun, Y., Bengio, Y., & Hinton, G. (2015). Deep learning. *Nature*, 521(7553), 436-444.

doi:10.1038/nature14539

Lei, L., Li, Z. H., Wu, J. T., Zhang, C. J., Zhu, Y. H., Chen, R. Q., . . . Yang, G. J. (2022). Extraction of Maize Leaf Base and Inclination Angles Using Terrestrial Laser Scanning (TLS) Data. *IEEE Transactions on Geoscience and Remote Sensing*, 60. doi:10.1109/tgrs.2022.3142205

Li, F., Hao, D., Zhu, Q., Yuan, K., Braghiere, R. K., He, L., . . . Chen, M. (2023). Vegetation clumping modulates global photosynthesis through adjusting canopy light environment. *Global Change Biology*, 29(3), 731-746. doi:10.1111/gcb.16503

Li, S., Fang, H., & Zhang, Y. (2023). Determination of the Leaf Inclination Angle (LIA) through Field and Remote Sensing Methods: Current Status and Future Prospects. *Remote Sensing*, 15(4). doi:10.3390/rs15040946

Liu, J., Skidmore, A. K., Wang, T., Zhu, X., Premier, J., Heurich, M., . . . Jones, S. (2019). Variation of leaf angle distribution quantified by terrestrial LiDAR in natural European beech forest. *ISPRS Journal of Photogrammetry and Remote Sensing*, 148, 208-220. doi:10.1016/j.isprsjprs.2019.01.005

Lugg, D. G., Youngman, V. E., & Hinze, G. (1981). LEAF AZIMUTHAL ORIENTATION OF SORGHUM IN 4 ROW DIRECTIONS. *Agronomy Journal*, 73(3), 497-500. doi:10.2134/agronj1981.00021962007300030022x

Mantilla-Perez, M. B., & Fernandez, M. G. S. (2017). Differential manipulation of leaf angle throughout the canopy: current status and prospects. *Journal of Experimental Botany*, 68(21-22), 5699-5717. doi:10.1093/jxb/erx378

McNeil, B. E., Pisek, J., Lepisk, H., & Flamenco, E. A. (2016). Measuring leaf angle distribution in broadleaf canopies using UAVs. *Agricultural and Forest Meteorology*, 218-219, 204-208.

doi:10.1016/j.agrformet.2015.12.058

Meunier, F., Visser, M. D., Shiklomanov, A., Dietze, M. C., Guzmán, Q. J. A., Sanchez-Azofeifa, G. A., . . . Verbeeck, H. (2022). Liana optical traits increase tropical forest albedo and reduce ecosystem productivity. *Global Change Biology*, 28(1), 227-244. doi:10.1111/gcb.15928

Muller-Linow, M., Pinto-Espinosa, F., Scharr, H., & Rascher, U. (2015). The leaf angle distribution of natural plant populations: assessing the canopy with a novel software tool. *Plant Methods*, 11. doi:10.1186/s13007-015-0052-z

Myneni, R., Asrar, G., Kanemasu, E., Lawlor, D., Impens, I. J. A., & meteorology, f. (1986). Canopy architecture, irradiance distribution on leaf surfaces and consequent photosynthetic efficiencies in heterogeneous plant canopies. Part 1. Theoretical considerations. *Agricultural and Forest Meteorology*, 37(3), 189-204.

Omasa, K., Hosoi, F., & Konishi, A. (2007). 3D lidar imaging for detecting and understanding plant responses and canopy structure. *Journal of Experimental Botany*, 58(4), 881-898. doi:10.1093/jxb/erl142

Oprea, S., Martinez-Gonzalez, P., Garcia-Garcia, A., Castro-Vargas, J. A., Orts-Escolano, S., Garcia-Rodriguez, J., & Argyros, A. (2022). A Review on Deep Learning Techniques for Video Prediction. *IEEE Transactions on Pattern Analysis and Machine Intelligence*, 44(6), 2806-2826. doi:10.1109/tpami.2020.3045007

Paulus, S. (2019). Measuring crops in 3D: using geometry for plant phenotyping. *Plant Methods*, 15(1). doi:10.1186/s13007-019-0490-0

Pisek, J., Ryu, Y., & Alikas, K. (2011). Estimating leaf inclination and G-function from leveled digital camera photography in broadleaf canopies. *Trees*, 25(5), 919-924. doi:10.1007/s00468-011-

532 0566-6

533 Qi, J., Xie, D., Li, L., Zhang, W., Mu, X., & Yan, G. (2019). Estimating Leaf Angle Distribution From
534 Smartphone Photographs. *IEEE Geoscience and Remote Sensing Letters*, 16(8), 1190-1194.
535 doi:10.1109/lgrs.2019.2895321

536 Raabe, K., Pisek, J., Sonnentag, O., & Annuk, K. (2015). Variations of leaf inclination angle distribution
537 with height over the growing season and light exposure for eight broadleaf tree species.
538 *Agricultural and Forest Meteorology*, 214, 2-11. doi:10.1016/j.agrformet.2015.07.008

539 Ren, S. Q., He, K. M., Girshick, R., & Sun, J. (2015, Dec 07-12). *Faster R-CNN: Towards Real-Time*
540 *Object Detection with Region Proposal Networks*. Paper presented at the 29th Annual
541 Conference on Neural Information Processing Systems (NIPS), Montreal, CANADA.

542 Ryu, Y., Sonnentag, O., Nilson, T., Vargas, R., Kobayashi, H., Wenk, R., & Baldocchi, D. D. (2010). How
543 to quantify tree leaf area index in an open savanna ecosystem: A multi-instrument and multi-
544 model approach. *Agricultural and Forest Meteorology*, 150(1), 63-76.
545 doi:10.1016/j.agrformet.2009.08.007

546 Sellers, P. J. (1985). CANOPY REFLECTANCE, PHOTOSYNTHESIS AND TRANSPIRATION.
547 *International Journal of Remote Sensing*, 6(8), 1335-1372. doi:10.1080/01431168508948283

548 Shell, G. S. G., Lang, A. R. G., & Sale, P. J. M. (1974). QUANTITATIVE MEASURES OF LEAF
549 ORIENTATION AND HELIOTROPIC RESPONSE IN SUNFLOWER, BEAN, PEPPER AND
550 CUCUMBER. *Agricultural Meteorology*, 13(1), 25-37. doi:10.1016/0002-1571(74)90062-4

551 Stovall, A. E. L., Masters, B., Fatoyinbo, L., & Yang, X. (2021). TLSLeAF: automatic leaf angle
552 estimates from single-scan terrestrial laser scanning. *New Phytologist*, 232(4), 1876-1892.
553 doi:10.1111/nph.17548

554 Toda, M., Ishihara, M. I., Doi, K., & Hara, T. (2022). Determination of species-specific leaf angle
 555 distribution and plant area index in a cool-temperate mixed forest from UAV and upward-
 556 pointing digital photography. *Agricultural and Forest Meteorology*, 325.
 557 doi:10.1016/j.agrformet.2022.109151
 558 Torralba, A., Russell, B. C., & Yuen, J. (2010). LabelMe: Online Image Annotation and Applications.
 559 *Proceedings of the Ieee*, 98(8), 1467-1484. doi:10.1109/jproc.2010.2050290
 560 Verhoeven, G. J. A. p. (2011). Taking computer vision aloft—archaeological three-dimensional
 561 reconstructions from aerial photographs with photoscan. *Archaeological Prospection*, 18(1), 67-
 562 73.
 563 Vicari, M. B., Pisek, J., & Disney, M. (2019). New estimates of leaf angle distribution from terrestrial
 564 LiDAR: Comparison with measured and modelled estimates from nine broadleaf tree species.
 565 *Agricultural and Forest Meteorology*, 264, 322-333. doi:10.1016/j.agrformet.2018.10.021
 566 Waeldechen, J., & Maeder, P. (2018). Plant Species Identification Using Computer Vision Techniques: A
 567 Systematic Literature Review. *Archives of Computational Methods in Engineering*, 25(2), 507-
 568 543. doi:10.1007/s11831-016-9206-z
 569 Wang, H., Zhang, W., Zhou, G., Yan, G., & Clinton, N. (2009). Image-based 3D corn reconstruction for
 570 retrieval of geometrical structural parameters. *International Journal of Remote Sensing*, 30(20),
 571 5505-5513.
 572 Wang, Y., & Fang, H. (2020). Estimation of LAI with the LiDAR Technology: A Review. *Remote Sensing*,
 573 12(20). doi:10.3390/rs12203457
 574 Westoby, M. J., Brasington, J., Glasser, N. F., Hambrey, M. J., & Reynolds, J. M. (2012). 'Structure-from-
 575 Motion' photogrammetry: A low-cost, effective tool for geoscience applications.

576 *Geomorphology*, 179, 300-314. doi:10.1016/j.geomorph.2012.08.021

577 Wilson, J. W. (1959). Analysis of the spatial distribution of foliage by two-dimensional point quadrats.

578 *New Phytologist*, 58(1), 92-99.

579 Xu, H., Blonder, B., Jodra, M., Malhi, Y., & Fricker, M. (2021). Automated and accurate segmentation

580 of leaf venation networks via deep learning. *New Phytologist*, 229(1), 631-648.

581 doi:10.1111/nph.16923

582 Yang, X., Li, R., Jablonski, A., Stovall, A., Kim, J., Yi, K., . . . Lerdau, M. (2023). Leaf angle as a leaf

583 and canopy trait: Rejuvenating its role in ecology with new technology. *Ecology Letters*, 26(6),

584 1005-1020. doi:10.1111/ele.14215

585 Zeng, Y., Hao, D., Park, T., Zhu, P., Huete, A., Myneni, R., . . . Chen, M. (2023). Structural complexity

586 biases vegetation greenness measures. *Nature Ecology & Evolution*, 7(11). doi:10.1038/s41559-

587 023-02187-6

588 Zheng, G., & Moskal, L. M. (2012). Leaf Orientation Retrieval From Terrestrial Laser Scanning (TLS)

589 Data. *IEEE Transactions on Geoscience and Remote Sensing*, 50(10), 3970-3979.

590 doi:10.1109/tgrs.2012.2188533

591 Zhu, B. L., Liu, F. S., Xie, Z. W., Guo, Y., Li, B. G., & Ma, Y. T. (2020). Quantification of light

592 interception within image-based 3-D reconstruction of sole and intercropped canopies over the

593 entire growth season. *Annals of Botany*, 126(4), 701-712. doi:10.1093/aob/mcaa046

594